

Measurement of $D^0 \rightarrow \pi l \nu(Kl\nu)$ and their form factors

K. Abe,⁹ K. Abe,⁴⁷ I. Adachi,⁹ H. Aihara,⁴⁹ K. Aoki,²³ K. Arinstein,² Y. Asano,⁵⁴
 T. Aso,⁵³ V. Aulchenko,² T. Aushev,¹³ T. Aziz,⁴⁵ S. Bahinipati,⁵ A. M. Bakich,⁴⁴
 V. Balagura,¹³ Y. Ban,³⁶ S. Banerjee,⁴⁵ E. Barberio,²² M. Barbero,⁸ A. Bay,¹⁹ I. Bedny,²
 U. Bitenc,¹⁴ I. Bizjak,¹⁴ S. Blyth,²⁵ A. Bondar,² A. Bozek,²⁹ M. Bračko,^{9, 21, 14}
 J. Brodzicka,²⁹ T. E. Browder,⁸ M.-C. Chang,⁴⁸ P. Chang,²⁸ Y. Chao,²⁸ A. Chen,²⁵
 K.-F. Chen,²⁸ W. T. Chen,²⁵ B. G. Cheon,⁴ C.-C. Chiang,²⁸ R. Chistov,¹³ S.-K. Choi,⁷
 Y. Choi,⁴³ Y. K. Choi,⁴³ A. Chuvikov,³⁷ S. Cole,⁴⁴ J. Dalseno,²² M. Danilov,¹³ M. Dash,⁵⁶
 L. Y. Dong,¹¹ R. Dowd,²² J. Dragic,⁹ A. Drutskoy,⁵ S. Eidelman,² Y. Enari,²³ D. Epifanov,²
 F. Fang,⁸ S. Fratina,¹⁴ H. Fujii,⁹ N. Gabyshev,² A. Garmash,³⁷ T. Gershon,⁹ A. Go,²⁵
 G. Gokhroo,⁴⁵ P. Goldenzweig,⁵ B. Golob,^{20, 14} A. Gorišek,¹⁴ M. Grosse Perdekamp,³⁸
 H. Guler,⁸ R. Guo,²⁶ J. Haba,⁹ K. Hara,⁹ T. Hara,³⁴ Y. Hasegawa,⁴² N. C. Hastings,⁴⁹
 K. Hasuko,³⁸ K. Hayasaka,²³ H. Hayashii,²⁴ M. Hazumi,⁹ T. Higuchi,⁹ L. Hinz,¹⁹ T. Hojo,³⁴
 T. Hokuue,²³ Y. Hoshi,⁴⁷ K. Hoshina,⁵² S. Hou,²⁵ W.-S. Hou,²⁸ Y. B. Hsiung,²⁸
 Y. Igarashi,⁹ T. Iijima,²³ K. Ikado,²³ A. Imoto,²⁴ K. Inami,²³ A. Ishikawa,⁹ H. Ishino,⁵⁰
 K. Itoh,⁴⁹ R. Itoh,⁹ M. Iwasaki,⁴⁹ Y. Iwasaki,⁹ C. Jacoby,¹⁹ C.-M. Jen,²⁸ R. Kagan,¹³
 H. Kakuno,⁴⁹ J. H. Kang,⁵⁷ J. S. Kang,¹⁶ P. Kapusta,²⁹ S. U. Kataoka,²⁴ N. Katayama,⁹
 H. Kawai,³ N. Kawamura,¹ T. Kawasaki,³¹ S. Kazi,⁵ N. Kent,⁸ H. R. Khan,⁵⁰
 A. Kibayashi,⁵⁰ H. Kichimi,⁹ H. J. Kim,¹⁸ H. O. Kim,⁴³ J. H. Kim,⁴³ S. K. Kim,⁴¹
 S. M. Kim,⁴³ T. H. Kim,⁵⁷ K. Kinoshita,⁵ N. Kishimoto,²³ S. Korpar,^{21, 14} Y. Kozakai,²³
 P. Krizan,^{20, 14} P. Krokovny,⁹ T. Kubota,²³ R. Kulasiri,⁵ C. C. Kuo,²⁵ H. Kurashiro,⁵⁰
 E. Kurihara,³ A. Kusaka,⁴⁹ A. Kuzmin,² Y.-J. Kwon,⁵⁷ J. S. Lange,⁶ G. Leder,¹²
 S. E. Lee,⁴¹ Y.-J. Lee,²⁸ T. Lesiak,²⁹ J. Li,⁴⁰ A. Limosani,⁹ S.-W. Lin,²⁸ D. Liventsev,¹³
 J. MacNaughton,¹² G. Majumder,⁴⁵ F. Mandl,¹² D. Marlow,³⁷ H. Matsumoto,³¹
 T. Matsumoto,⁵¹ A. Matyja,²⁹ Y. Mikami,⁴⁸ W. Mitaroff,¹² K. Miyabayashi,²⁴ H. Miyake,³⁴
 H. Miyata,³¹ Y. Miyazaki,²³ R. Mizuk,¹³ D. Mohapatra,⁵⁶ G. R. Moloney,²² T. Mori,⁵⁰
 A. Murakami,³⁹ T. Nagamine,⁴⁸ Y. Nagasaka,¹⁰ T. Nakagawa,⁵¹ I. Nakamura,⁹
 E. Nakano,³³ M. Nakao,⁹ H. Nakazawa,⁹ Z. Natkaniec,²⁹ K. Neichi,⁴⁷ S. Nishida,⁹
 O. Nitoh,⁵² S. Noguchi,²⁴ T. Nozaki,⁹ A. Ogawa,³⁸ S. Ogawa,⁴⁶ T. Ohshima,²³ T. Okabe,²³
 S. Okuno,¹⁵ S. L. Olsen,⁸ Y. Onuki,³¹ W. Ostrowicz,²⁹ H. Ozaki,⁹ P. Pakhlov,¹³ H. Palka,²⁹
 C. W. Park,⁴³ H. Park,¹⁸ K. S. Park,⁴³ N. Parslow,⁴⁴ L. S. Peak,⁴⁴ M. Pernicka,¹²
 R. Pestotnik,¹⁴ M. Peters,⁸ L. E. Piilonen,⁵⁶ A. Poluektov,² F. J. Ronga,⁹ N. Root,²
 M. Rozanska,²⁹ H. Sahoo,⁸ M. Saigo,⁴⁸ S. Saitoh,⁹ Y. Sakai,⁹ H. Sakamoto,¹⁷
 H. Sakaue,³³ T. R. Sarangi,⁹ M. Satapathy,⁵⁵ N. Sato,²³ N. Satoyama,⁴² T. Schietinger,¹⁹
 O. Schneider,¹⁹ P. Schönmeier,⁴⁸ J. Schümann,²⁸ C. Schwanda,¹² A. J. Schwartz,⁵
 T. Seki,⁵¹ K. Senyo,²³ R. Seuster,⁸ M. E. Sevier,²² T. Shibata,³¹ H. Shibuya,⁴⁶
 J.-G. Shiu,²⁸ B. Shwartz,² V. Sidorov,² J. B. Singh,³⁵ A. Somov,⁵ N. Soni,³⁵ R. Stamen,⁹
 S. Stanič,³² M. Starič,¹⁴ A. Sugiyama,³⁹ K. Sumisawa,⁹ T. Sumiyoshi,⁵¹ S. Suzuki,³⁹
 S. Y. Suzuki,⁹ O. Tajima,⁹ N. Takada,⁴² F. Takasaki,⁹ K. Tamai,⁹ N. Tamura,³¹
 K. Tanabe,⁴⁹ M. Tanaka,⁹ G. N. Taylor,²² Y. Teramoto,³³ X. C. Tian,³⁶ K. Trabelsi,⁸
 Y. F. Tse,²² T. Tsuboyama,⁹ T. Tsukamoto,⁹ K. Uchida,⁸ Y. Uchida,⁹ S. Uehara,⁹

T. Uglov,¹³ K. Ueno,²⁸ Y. Unno,⁹ S. Uno,⁹ P. Urquijo,²² Y. Ushiroda,⁹ G. Varner,⁸
 K. E. Varvell,⁴⁴ S. Villa,¹⁹ C. C. Wang,²⁸ C. H. Wang,²⁷ M.-Z. Wang,²⁸ M. Watanabe,³¹
 Y. Watanabe,⁵⁰ L. Widhalm,¹² C.-H. Wu,²⁸ Q. L. Xie,¹¹ B. D. Yabsley,⁵⁶ A. Yamaguchi,⁴⁸
 H. Yamamoto,⁴⁸ S. Yamamoto,⁵¹ Y. Yamashita,³⁰ M. Yamauchi,⁹ Heyoung Yang,⁴¹
 J. Ying,³⁶ S. Yoshino,²³ Y. Yuan,¹¹ Y. Yusa,⁴⁸ H. Yuta,¹ S. L. Zang,¹¹ C. C. Zhang,¹¹
 J. Zhang,⁹ L. M. Zhang,⁴⁰ Z. P. Zhang,⁴⁰ V. Zhilich,² T. Ziegler,³⁷ and D. Zürcher¹⁹

(The Belle Collaboration)

¹*Aomori University, Aomori*

²*Budker Institute of Nuclear Physics, Novosibirsk*

³*Chiba University, Chiba*

⁴*Chonnam National University, Kwangju*

⁵*University of Cincinnati, Cincinnati, Ohio 45221*

⁶*University of Frankfurt, Frankfurt*

⁷*Gyeongsang National University, Chinju*

⁸*University of Hawaii, Honolulu, Hawaii 96822*

⁹*High Energy Accelerator Research Organization (KEK), Tsukuba*

¹⁰*Hiroshima Institute of Technology, Hiroshima*

¹¹*Institute of High Energy Physics,*

Chinese Academy of Sciences, Beijing

¹²*Institute of High Energy Physics, Vienna*

¹³*Institute for Theoretical and Experimental Physics, Moscow*

¹⁴*J. Stefan Institute, Ljubljana*

¹⁵*Kanagawa University, Yokohama*

¹⁶*Korea University, Seoul*

¹⁷*Kyoto University, Kyoto*

¹⁸*Kyungpook National University, Taegu*

¹⁹*Swiss Federal Institute of Technology of Lausanne, EPFL, Lausanne*

²⁰*University of Ljubljana, Ljubljana*

²¹*University of Maribor, Maribor*

²²*University of Melbourne, Victoria*

²³*Nagoya University, Nagoya*

²⁴*Nara Women's University, Nara*

²⁵*National Central University, Chung-li*

²⁶*National Kaohsiung Normal University, Kaohsiung*

²⁷*National United University, Miao Li*

²⁸*Department of Physics, National Taiwan University, Taipei*

²⁹*H. Niewodniczanski Institute of Nuclear Physics, Krakow*

³⁰*Nippon Dental University, Niigata*

³¹*Niigata University, Niigata*

³²*Nova Gorica Polytechnic, Nova Gorica*

³³*Osaka City University, Osaka*

³⁴*Osaka University, Osaka*

³⁵*Panjab University, Chandigarh*

³⁶*Peking University, Beijing*

³⁷*Princeton University, Princeton, New Jersey 08544*

³⁸*RIKEN BNL Research Center, Upton, New York 11973*

- ³⁹*Saga University, Saga*
⁴⁰*University of Science and Technology of China, Hefei*
⁴¹*Seoul National University, Seoul*
⁴²*Shinshu University, Nagano*
⁴³*Sungkyunkwan University, Suwon*
⁴⁴*University of Sydney, Sydney NSW*
⁴⁵*Tata Institute of Fundamental Research, Bombay*
⁴⁶*Toho University, Funabashi*
⁴⁷*Tohoku Gakuin University, Tagajo*
⁴⁸*Tohoku University, Sendai*
⁴⁹*Department of Physics, University of Tokyo, Tokyo*
⁵⁰*Tokyo Institute of Technology, Tokyo*
⁵¹*Tokyo Metropolitan University, Tokyo*
⁵²*Tokyo University of Agriculture and Technology, Tokyo*
⁵³*Toyama National College of Maritime Technology, Toyama*
⁵⁴*University of Tsukuba, Tsukuba*
⁵⁵*Utkal University, Bhubaneswer*
⁵⁶*Virginia Polytechnic Institute and State University, Blacksburg, Virginia 24061*
⁵⁷*Yonsei University, Seoul*

Abstract

Using a data sample of 282 fb^{-1} collected by the Belle experiment at the KEKB e^+e^- collider, we study $D^0 \rightarrow \pi^- \ell^+ \nu$ and $D^0 \rightarrow K^- \ell^+ \nu$ decays ($\ell = \mu, e$) in e^+e^- annihilation. We identify $D^{*+} \rightarrow D^0 \pi^+$ decays by using the mass of the system recoiling against a fully reconstructed tag-side D^* or D meson, allowing for additional primary mesons from fragmentation. Using a novel global reconstruction method that provides very good resolution in neutrino momentum and in $q^2 = (p_\ell + p_\nu)^2$, we reconstructed $D^0 \rightarrow \pi^- \ell^+ \nu$ and $D^0 \rightarrow K^- \ell^+ \nu$ decays. From these events we measured the branching fraction ratios $BR(D^0 \rightarrow \pi e \nu)/BR(D^0 \rightarrow K e \nu) = 0.0809 \pm 0.0080 \pm 0.0032$ and $BR(D^0 \rightarrow \pi \mu \nu)/BR(D^0 \rightarrow K \mu \nu) = 0.0677 \pm 0.0078 \pm 0.0047$, and the semileptonic form factor ratio $f_+(D^0 \rightarrow \pi^- \ell^+ \nu)^2/f_+(D^0 \rightarrow K^- \ell^+ \nu)^2 \cdot |V_{cd}|^2/|V_{cs}|^2|_{q^2=0} = 0.041 \pm 0.003 \pm 0.004$, where the errors are statistical and systematic, respectively.

PACS numbers: 13.20.Fc, 14.40.Lb, 13.66.Bc

INTRODUCTION

Semileptonic decays of heavy-to-light mesons are of special interest since they are well suited to determine CKM matrix elements such as V_{ub} , V_{cd} , V_{cs} . However, some of these parameters — in particular V_{ub} — are not yet measured with satisfactory precision. The hadronic current in the semileptonic decays of B and D mesons is parametrized through form factors that depend on the invariant mass q^2 of the exchanged W boson. In the past, the form factors for the two decays, $f_B(q^2)$ and $f_D(q^2)$, have been calculated in the quenched approximation of lattice QCD[1]. Results from unquenched calculations have only recently become available [2–4]. Imprecise knowledge of form factors is the main source of uncertainty in the extraction of the CKM matrix elements in semileptonic decays [5]. When $|V_{ub}|$ is measured via $B^0 \rightarrow \pi^- \ell^+ \nu$, one uses the form factor $f_B(q^2)$; similarly, for $|V_{cd}|$ via $D^0 \rightarrow \pi^- \ell^+ \nu$, the form factor $f_D(q^2)$ is used. In the ratio of these form factors some of the theoretical uncertainties cancel [6]. Accurate information on the form factor $f_D(q^2)$ from the decay $D^0 \rightarrow \pi^- \ell^+ \nu$ can be related to the measurement of $f_B(q^2)$ and hence also $|V_{ub}|$ and can test the validity of an effective pole ansatz [7] or the ISGW2 model [8]. The semileptonic form factor has also been investigated by CLEO [9], FOCUS [10], BES [11], and CLEO-c [12].

In addition to the semileptonic decay $D^0 \rightarrow \pi^- \ell^+ \nu$ we also investigate the channel $D^0 \rightarrow K^- \ell^+ \nu$, which has much less background and provides about 10 times higher statistics. From a study of the two semileptonic channels we can evaluate the relative branching fractions of these decay modes.

DATA AND MONTE CARLO SETS

The data collected by the Belle detector at the center of mass (CM) energy of 10.58 GeV ($\Upsilon(4S)$) and 60 MeV below that, corresponding to a total integrated luminosity of 282 fb⁻¹, was used. The Belle detector is a large-solid-angle magnetic spectrometer that consists of a multi-layer silicon vertex detector (SVD), a 50-layer central drift chamber (CDC), an array of aerogel threshold Čerenkov counters (ACC), a barrel-like arrangement of time-of-flight scintillation counters (TOF), and an electromagnetic calorimeter (ECL) comprised of CsI(Tl) crystals located inside a superconducting solenoid coil that provides a 1.5 T magnetic field. An iron flux-return located outside of the coil is instrumented to detect K_L^0 mesons and to identify muons (KLM). The detector is described in detail elsewhere [13]. Two different inner detector configurations were used. For the first sample corresponding to roughly half the statistics, a 2.0 cm radius beampipe and a 3-layer silicon vertex detector were used; for the second sample, a 1.5 cm radius beampipe, a 4-layer silicon detector and a small-cell inner drift chamber were used [14].

Simulated Monte Carlo (MC) events were used for checks of the reconstruction method and background determination. The MC includes $\Upsilon(4S) \rightarrow B\bar{B}$ and continuum ($q\bar{q}$, where $q = c, s, u, d$) events, generated using the QQ generator [15] and processed through a complete GEANT-based simulation [16] of the Belle detector. We refer to this as the generic MC sample. We also use MC samples of signal events for optimisation of selection criteria and signal reconstruction efficiency determination.

ANALYSIS STRATEGY AND EVENT SELECTION

To measure semileptonic decays $D^0 \rightarrow h^- \ell^+ \nu$ ($h = \pi$ or K , $\ell = e$ or μ), we consider event topologies of the type $e^+e^- \rightarrow D^{(*)}D^*X$, where the $D^{(*)}$ system is referred to as the tag side, the D^* system is referred to as the signal side, and X denotes additional mesons including π^0 , π^\pm and K^\pm (Fig. 1). We use a global reconstruction technique that requires all the final state particles in the event, with the exception of the neutrino from the signal D semileptonic decay, to be detected. In this paper, the reconstruction of charge conjugate modes is implied throughout. We found in agreement with [17] (which studied the case of no additional particles) that the $e^+e^- \rightarrow D\bar{D}X$ cross section is negligible, while for DD^* and D^*D^* the cross sections are so large that in spite of decreasing reconstruction efficiencies with increasing number of fragmentation particles, statistics can be significantly enhanced by our reconstruction method. Instead of reconstructing decay chains step-by-step by applying intermediate selection criteria, all possible decay chains matching certain patterns (event topology and loose mass windows) are considered, leading to a possibly large number of intermediate combinations in a single event that is pruned at later steps in the reconstruction chain. This strategy in many cases automatically solves the problem of ambiguities that would arise in a sequential reconstruction, and also allows looser selection criteria for individual particles, thus giving a higher reconstruction efficiency. Appropriate selection criteria, described below, are applied to select D^0 semileptonic decays. The case of multiple signal candidates is treated by assigning each remaining candidate the same weight.

Tracks are detected with the CDC and SVD. They are required to have at least one associated hit in the SVD and an impact parameter with respect to the interaction point in the radial direction of less than 2 cm and in the beam direction of less than 4 cm. Tracks are also required to have momentum in the laboratory frame greater than 100 MeV/ c . A likelihood ratio for a given track to be a kaon or pion was obtained by utilising specific ionisation energy loss measurements made with the CDC, light yield measurements from the ACC, and time of flight information from the TOF. Lepton candidates were required to have momentum larger than 500 MeV/ c . For electron identification we use position, cluster energy, shower shape in the ECL, combined with track momentum and dE/dx measurements in the CDC and hits in the ACC. For muon identification, we extrapolate the CDC track to the KLM and compare the measured range and transverse deviation in the KLM with the expected values. Photons are required to have energies in the laboratory frame greater than 50 MeV. Neutral pion candidates were reconstructed using $\gamma\gamma$ pairs with invariant mass within ± 10 MeV/ c^2 of the nominal π^0 mass. These candidates are also subject to a mass constrained vertex fit, assuming they arise from the interaction point, for which the confidence level is required to be greater than 0.1.

We reconstruct tag-side D^\pm and D^0 candidates in the channels $D^\pm \rightarrow K^\pm n\pi$ and $D^0 \rightarrow K^\pm n\pi$ where the pions can be charged or neutral, and $n = 1, 2, 3$. Depending on the channel the candidate mass window varies in the range 5 – 60 MeV/ c^2 around the nominal D mass, corresponding to $\pm 5\sigma$. These candidates undergo a mass constrained vertex fit and we retain only those for which the fit is successful. An attempt is then made to reconstruct D^* candidates on the tag side via $D^{*+} \rightarrow D^0\pi^+$, $D^{*+} \rightarrow D^+\pi^0$, $D^{*0} \rightarrow D^0\pi^0$, $D^{*0} \rightarrow D^0\gamma$, and charge conjugate modes. The mass window around the nominal D^* mass is 5 (20) MeV/ c^2 for the non-radiative (radiative) mode. We require a successful mass constrained vertex fit of the D^* candidate. At this stage of the reconstruction we either have a fully reconstructed $D^{\pm 0*}$ or $D^{\pm 0}$ candidate on the tag side.

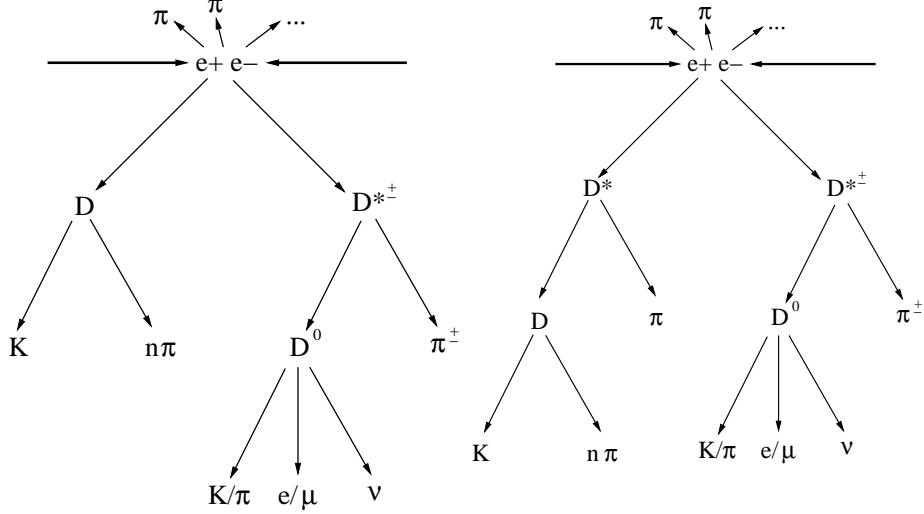


FIG. 1: Scheme of reconstructed event topology. Left: DD^* events- $D(\text{tag})D^{*\pm}(\text{signal})$. Right: D^*D^* events- $D^*(\text{tag})D^{*\pm}(\text{signal})$.

Along with possible additional primary mesons, we search for signal side $D^{*\pm}$ in the recoil of the tag side: the 4-momentum of the $D^{*\pm}$ candidate ($p_{D^{*\pm}\text{cand}}$) is reconstructed using the 4-momenta of the beams (p_{beam}), that of the tag-side $p_{D^{(*)}}$ and of the primary meson system p_X as $p_{D^{*\pm}\text{cand}} = p_{\text{beam}} - p_{D^{(*)}} - p_X$. The accuracy of the $D^{*\pm}$ candidate momentum is improved by applying a mass constrained vertex fit to the recoil particle. For candidates where the fit to D^* has a confidence level probability larger than 0.1%, an analogous fit is repeated for a recoil D^0 from $D^{*\pm} \rightarrow D^0\pi_s^\pm$ decay. The charge of the slow pion π_s is required to be the same as that of the kaon arising from the tag side D . The small available phase space for $D^{*+} \rightarrow D^0\pi^+$ in addition to the mass constraint leads to a very sharp peak in the D^0 candidate mass distribution (Fig. 2). Finally, neutrino candidates in the semileptonic D^0 decay are identified on the basis of the missing mass squared m_{miss}^2 , where the missing 4-momentum is calculated as

$$p_{\text{miss}} = p_{D,\text{signal-side}} - p_{K/\pi} - p_{e/\mu}. \quad (1)$$

Neutrino candidates are retained if their CM energy is greater than 100 MeV, if the remaining photon candidates not used in the reconstruction have an energy sum in the CM frame of less than 700 MeV and finally if the charges of the lepton and the slow pion are the same.

The signal region for D^0 semileptonic decays is defined as $|m_{\text{miss}}|^2 < 0.05 \text{ GeV}^2/c^4$. Our method yields a good resolution on the neutrino mass and the momentum transfer q^2 by applying a mass constrained vertex fit for neutrinos. The latter is found to be $\sigma_{q^2} = 0.0145 \pm 0.0007 \text{ GeV}^2/c^2$ in MC signal events. Although in the fit particles by default are assumed to originate from the interaction region, the influence of the D^0 decay distance on the reconstructed q^2 value has been corrected for by shifting the D^0 vertex in the direction of the fitted D^0 momentum by a distance corresponding to the mean lifetime of the meson. No significant change of the q^2 value or resolution has been observed.

For future reference the multiplicity of an event is defined as the total number of π^\pm , π^0 and K^\pm mesons not assigned as decay products of the tag-side D or signal-side D^* .

After the selection 75% of remaining events have one candidate while a negligible fraction have greater than three candidates. Multiple candidates in events are mainly due to an interchange of particles within a particular decay chain, each is assigned equal weight within an event. A possible bias in the measurement of q^2 that may arise due to events where the lepton and meson are interchanged, a double mis-assignment, was checked with candidate $D^0 \rightarrow K^- \ell^+ \nu$ events, and found to be negligible.

BACKGROUND STUDIES AND BACKGROUND SUBTRACTION

Non D^0 -events and events with badly reconstructed D^0

Fig. 2 (top) shows the composition of the inclusive signal side D^0 invariant mass spectrum for generic MC, where the reconstruction of the neutrino candidate has yet to be performed. The generic MC sample consists of events that may contain D^0 , namely $\Upsilon(4S) \rightarrow B\bar{B}$ (*bottom*), $e^+e^- \rightarrow c\bar{c}$ events (*charm*), and a pure background sample of $e^+e^- \rightarrow q\bar{q}$ where $q = u, d, s$ (*uds*). Signal events have been distinguished according to MC generator information. Most of the background comes either from *uds* or from a misreconstruction of the D^0 . There is also a small contribution from the B -meson samples ($\approx 1.4\%$). Performing the full signal side reconstruction and applying all signal selecting requirements as described above reduced the relative background level to approximately 1% (10%) for $D^0 \rightarrow K^- \ell^+ \nu$ ($D^0 \rightarrow \pi^- \ell^+ \nu$), with the remaining background dominated by charm events with an incorrectly reconstructed D^0 . Several constrained fits that are performed in the reconstruction may make background events look more like signal (peaking backgrounds). This possibility has been investigated in the generic MC sample and no peaking of the background has been observed.

The background is estimated by taking the D^0 mass spectrum from a wrong-sign D^0 sample defined by opposite charges of the kaon from the tag-side D decay and the signal-side slow pion. The right- and wrong-sign D^0 mass spectra in generic MC are shown in Fig.2. Subtracting the wrong-sign D^0 mass distribution from the right-sign distribution results in almost complete cancellation of the background in the latter, implying that the non- D^0 background is dominantly charge-uncorrelated [23]. The bottom plot in Fig. 2 shows that D^0 candidates are also found in the wrong sign sample, with a yield approximately 10% of that in the right-sign sample.

Since the charge-correlated non- D^0 background is very small, only the charge-uncorrelated part is considered, and a systematic error is assigned for the charge-correlated part, defined as the difference of background in right- and wrong-sign, equal to its relative contribution as observed in MC. To subtract the small component of real D^0 's in the wrong-sign sample, we use the difference of the right- and wrong-sign sample as model of the true D^0 signal shape, and fit this to the wrong-sign sample. For this purpose, the wrong-sign background is approximated as a second order polynomial in the signal region, $1.862 - 1.867$ GeV/c^2 . The fitted wrong-sign D^0 component is subtracted, and the remaining distribution is used to represent the shape of the non- D^0 background. It is normalized to the data in the sideband $1.84 - 1.85$ GeV/c^2 of the D^0 mass spectrum thus obtaining the amount of non- D^0 background in the signal region (which is defined as the region selected by the criterion on the confidence level of the D^0 mass-constrained vertex fit). This method is confirmed with generic MC (using $D^0 \rightarrow \pi^- \ell^+ \nu$ selection criteria): the measured background is 6.5 ± 1.4 events, compared to the true value of 6.

Yields of the measured non- D^0 background are given in Table I. The systematic error

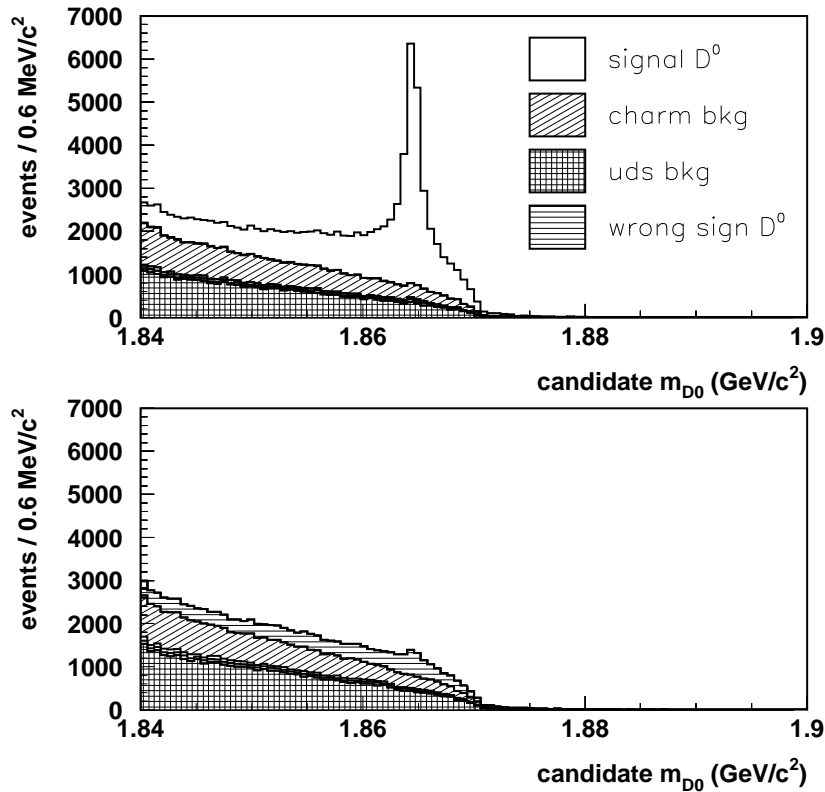


FIG. 2: Inclusive D^0 mass spectrum in generic MC events for right- (top) and wrong-sign (bottom) samples. The invariant mass shown is that prior to the D^0 mass-constrained fit.

for this measurement consists of a statistical part (from background shape and sideband statistics), a part due to the subtraction of wrong-sign signal events, the effect of the small component of charge-correlated background measured with MC, and of possible bias of the background shape due to selection criteria, which has been estimated by comparing the measurement with the result using loose selection criteria, *i.e.*, only those selecting D^0 (without the requirement on the confidence level of the mass constrained fit). Individual uncertainties are listed in Table II.

Background from semileptonic decays with a misidentified or undetected meson

The background from real semileptonic decays, with an incorrectly identified meson or additional mesons lost in reconstruction, is highly suppressed by the good neutrino mass resolution (see measurements below). For the signal channel $D^0 \rightarrow \pi^- \ell^+ \nu$, there are backgrounds from $D^0 \rightarrow K^- \ell^+ \nu$, $D^0 \rightarrow \rho^- \ell^+ \nu$ (with $\rho^- \rightarrow \pi^- \pi^0$), $D^0 \rightarrow K^{*-} \ell^+ \nu$ (with $K^{*-} \rightarrow K^0 \pi^-$), as well as non-resonant decays into the latter two final states. The most significant background is due to $D^0 \rightarrow K^- \ell^+ \nu$ since the branching fraction is approximately 10 times larger than the signal.

For the signal channel $D^0 \rightarrow K^- \ell^+ \nu$, it was verified using MC that backgrounds from $D^0 \rightarrow \pi^- \ell^+ \nu$ and $D^0 \rightarrow \rho^- \ell^+ \nu$ are completely negligible due to the much smaller branching fractions. The latter channel is suppressed even further by the selection criteria, due to the additional missing momentum taken by the π^0 from $\rho^- \rightarrow \pi^- \pi^0$. The channel $D^0 \rightarrow K^{*-} \ell^+ \nu$ contributes a small amount via $K^{*-} \rightarrow K^- \pi^0$.

To measure the semileptonic background in the $D^0 \rightarrow \pi^- \ell^+ \nu$ sample from $D^0 \rightarrow K^- \ell^+ \nu$, the distribution of simulated $D^0 \rightarrow K^- \ell^+ \nu$ decays that pass the selection criteria was normalized to the signal peak of the $D^0 \rightarrow K^- \ell^+ \nu$ data events, then multiplied by the expected misidentification probability for kaons to be identified as pions. The misidentification rates were corrected for known differences with real data, measured with a dedicated D^* sample in bins of meson momentum and polar angle. The remaining contribution of $D^0 \rightarrow K^{*-} \ell^+ \nu$ and $D^0 \rightarrow \rho^- \ell^+ \nu$ was obtained from MC and normalized in the region $m_\nu^2 > 0.3 \text{ GeV}^2/c^4$. For $D^0 \rightarrow K^- \ell^+ \nu$, the only semileptonic background stems from $D^0 \rightarrow K^{*-} \ell^+ \nu$, which was determined with normalized MC as described above.

The systematic error in the estimate of the semileptonic background includes uncertainties due to MC statistics, in the misidentification probability correction and in the ratio of K^* and ρ contributions. Yields of the semileptonic background are shown in Table I; their contributions to the systematic error are listed in Table II.

Hadronic D^0 -decays with fake leptons

As the fake rate for muons is about an order of magnitude larger than that for electrons, the background from hadronic D^0 -decays with fake muons is much more significant. To study and further categorize this kind of background, it is useful to look once more at wrong-sign data, in this case the lepton has opposite charge to that of the slow pion. The large $D^0 \rightarrow K^- \pi^+$ channel can contribute to the background for $D^0 \rightarrow K^- \ell^+ \nu$ (right-sign), and $D^0 \rightarrow \pi^- \ell^+ \nu$ (wrong-sign) [24]. The wrong mass hypothesis allows some energy for a possible neutrino candidate, but with the additional requirement $E_\nu \geq 100 \text{ MeV}$ this background is removed for both cases. However, in the decay $D^0 \rightarrow K^- \pi^+ \pi^0$ the π^0 may have enough momentum to fake a neutrino that passes the E_ν selection criterion. For $D^0 \rightarrow K^- \ell^+ \nu$ ($D^0 \rightarrow \pi^- \ell^+ \nu$), this background contributes to the right-sign (wrong-sign) sample. The background channel $D^0 \rightarrow \pi^- \pi^+ \pi^0$ contributes equally to right and wrong sign samples.

To measure the shapes of these backgrounds, special samples are used wherein identified kaons and pions are intentionally misidentified as leptons. As these raw shapes also contain some amount of non- D^0 background, the same procedure as described in the previous section is used to measure and subtract this part. A linear combination of the shapes of intentionally misidentified kaons and pions is fitted to the measured m_ν^2 distribution of the wrong-sign sample (see Fig. 3). Assuming that the K^\pm and π^\pm misidentification rates do not depend on the charge of the slow pion, the same amount of background contributes to the wrong-sign and the right-sign samples. Since the statistics for wrong-sign data samples in the $D^0 \rightarrow K^- \ell^+ \nu$ channel is very small, we use the measured fake-rates in $D^0 \rightarrow \pi^- \ell^+ \nu$ for the kaon modes as well. Numerical results can be found in Table I.

It has been checked using the generic MC sample that the shape of the background is relatively insensitive to the differences in the kinematics of correctly identified and misidentified mesons; the possible small differences have been included in the systematic error (see Table II). The statistical error in the fits to the wrong-sign sample is included in the

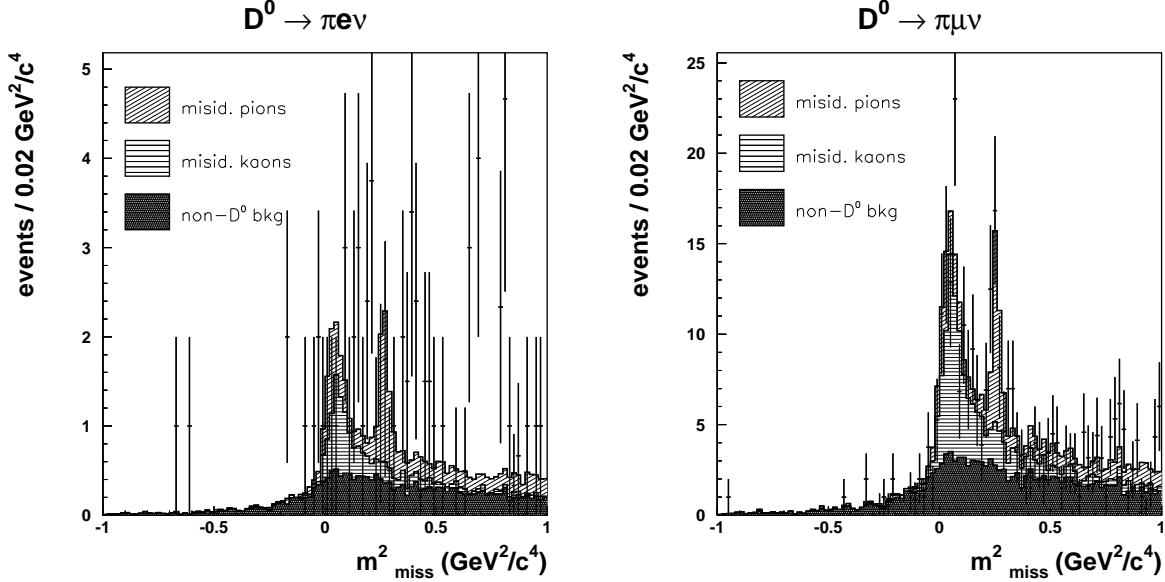


FIG. 3: Fitted hadronic background shapes for the pion channels in the wrong-sign data sample (defined by opposite charges of the slow pion and the lepton); the two prominent peaks correspond to background from $D^0 \rightarrow K^- \pi^+ \pi^0$ (lower m_{miss}^2) and $D^0 \rightarrow K^0 \pi^+ \pi^-$ (higher m_{miss}^2)

systematic uncertainties as well.

Fig. 4 shows the measured backgrounds and the signal for all four semileptonic decays of the D^0 . Table I gives the yields for the background sources. The MC sample was used to check that all the significant background components are taken into account using the above described methods.

BRANCHING RATIOS OF SEMILEPTONIC DECAYS OF D^0

After background subtraction, the yields for the four studied semileptonic D^0 decay modes are given in Table I. The contributions to systematic uncertainties for each individual background source are listed in Table II.

The dependence of signal yields on the multiplicity has been studied with generic MC. Although the efficiency decreases as the multiplicity of the event increases, the ratio ϵ_π/ϵ_K , where ϵ_π (ϵ_K) is the efficiency of the $D^0 \rightarrow \pi^- \ell^+ \nu$ ($K^- \ell^+ \nu$) channel, is flat (Fig. 5, $\chi^2/ndf = 0.84$). The observed multiplicity in the data is slightly different from the simulated one. In order to estimate the systematic error due to this difference, we reweighted the simulated efficiencies according to the data multiplicity distribution. Since the $D^0 \rightarrow \pi^- \ell^+ \nu$ and $D^0 \rightarrow K^- \ell^+ \nu$ decay samples are topologically very similar, we used a sample of events where only the selection on the signal-side D^0 meson was applied. The efficiency ratio for the reweighted inclusive D^0 sample and the $D^0 \rightarrow K^- \ell^+ \nu$ sample compared to the simulated ratio yields a correction factor of 0.981 ± 0.028 . Since this is compatible with unity, no correction is applied to the efficiency ratio; instead, the uncertainty of this factor is included in the systematic error. The values for the efficiencies, corrected and averaged over multiplicity, are listed in Table III.

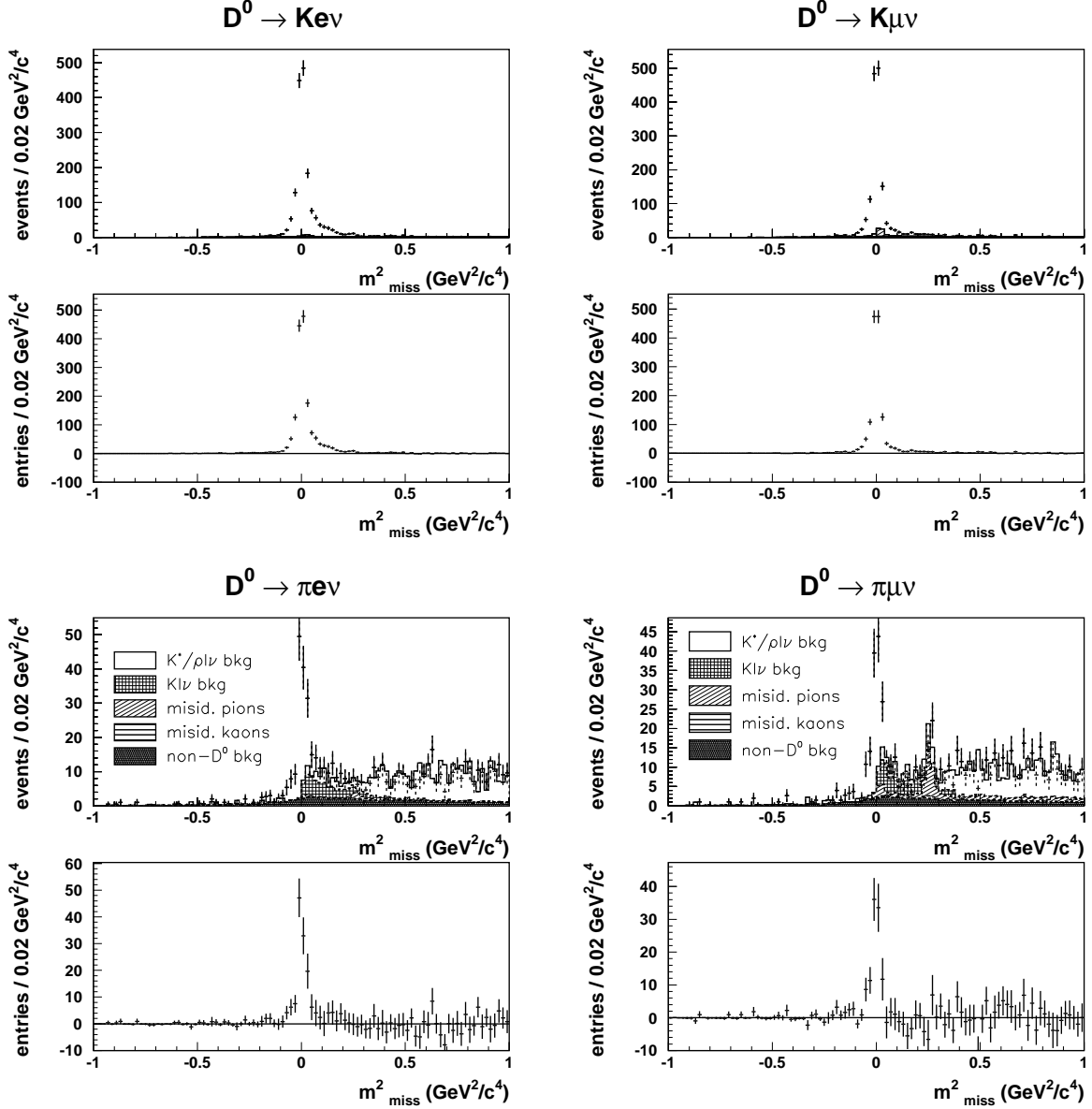


FIG. 4: Decomposition of background for the four semileptonic channels. In each case the lower plot shows the background-subtracted signal.

Using these efficiencies, the relative branching ratios are obtained and are shown in Table IV. We have divided our data sample into low- and high-multiplicities sets of three or fewer and four or more pions (kaons), respectively, and found consistent results. The results are also in agreement with recent measurements from CLEO [9, 12] and FOCUS [20]

q^2 -DISTRIBUTION

The square of the four-momentum transfer q in the semileptonic channel is given by $q^2 = (p_\nu + p_\ell)^2$, where p is the four momentum of the specified particle. The good neutrino

channel	$K^- e^+ \nu$	$K^- \mu^+ \nu$	$\pi^- e^+ \nu$	$\pi^- \mu^+ \nu$
total yield	1349	1333	152	141
signal yield	1318	1248	126	107
statistical error	37	37	12	12
total systematic error	7	24	2.6	6
non- D^0 background	12.6 ± 2.2	12.4 ± 4.8	12.3 ± 2.2	11.5 ± 4.5
semileptonic background	6.7 ± 2.6	10.0 ± 2.5	11.7 ± 1.2	12.6 ± 1.9
hadronic background	11.9 ± 5.6	62.1 ± 23.9	1.8 ± 0.7	9.7 ± 3.7

TABLE I: Final signal yields and backgrounds.

channel	$K^- e^+ \nu$	$K^- \mu^+ \nu$	$\pi^- e^+ \nu$	$\pi^- \mu^+ \nu$
non-D^0 background:				
statistics of background shape	4.2%	8.1%	6.6%	13.4%
subtraction of wrong sign	1.0%	1.0%	1.3%	1.3%
charge correlated background	6.3%	13.1%	5.5%	11.9%
shape minimum bias	15.7%	35.2%	15.3%	34.1%
sum in quadrature	17.5%	38.4%	17.6%	38.5%
semileptonic background:				
statistics MC samples	39%	25%	9.7%	14.4%
fake rates ratio MC/data	4%	3%	2.9%	3.2%
uncertainty of $K^{*-} \ell^+ \nu / \rho^- \ell^+ \nu$	< 1%	< 1%	1.4%	1.7%
sum in quadrature	39.2%	25.2%	10.2%	14.8%
hadronic background:				
fit of wrong sign shapes, mis-id kaons	2%	1%	3%	3%
fit of wrong sign shapes, mis-id pions	33%	16%	35%	23%
bias of background shapes	33%	35%	11%	30%
sum in quadrature	46.7%	38.5%	36.8%	37.9%

TABLE II: Relative systematic errors on the amount of respective backgrounds.

resolution leads also to a very good resolution for q^2 , described by a double Gaussian with a common mean of $0.00061 \pm 0.00031 \text{ GeV}^2/c^2$ and widths of $\sigma_1 = 0.0109 \pm 0.0005 \text{ GeV}^2/c^2$, $\sigma_2 = 0.0401 \pm 0.0026 \text{ GeV}^2/c^2$, the fraction of the wider Gaussian being 0.14 ± 0.02 . No unfolding of the q^2 distributions is needed since these resolutions are much less than the bin widths used. The dependence of q^2 resolution on different multiplicities is small; $\sigma(q^2)$ lies in the range 0.0095 to $0.0121 \text{ GeV}^2/c^2$ (with a $\sim 10\%$ uncertainty) for pion/kaon multiplicities between 0 and 8. The background subtraction in the determination of the q^2 distribution is performed using the method described earlier. The results are shown in Fig. 6 and are consistent with MC.

channel	$K^- e^+ \nu$	$K^- \mu^+ \nu$
efficiency	$(0.369 \pm 0.005 \pm 0.010)\%$	$(0.350 \pm 0.005 \pm 0.010)\%$
channel	$\pi^- e^+ \nu$	$\pi^- \mu^+ \nu$
efficiency	$(0.436 \pm 0.006 \pm 0.012)\%$	$(0.443 \pm 0.006 \pm 0.012)\%$

TABLE III: Efficiencies for semileptonic decay channels, averaged over multiplicity; errors shown are due to MC statistics and multiplicity dependence, as described in the text.

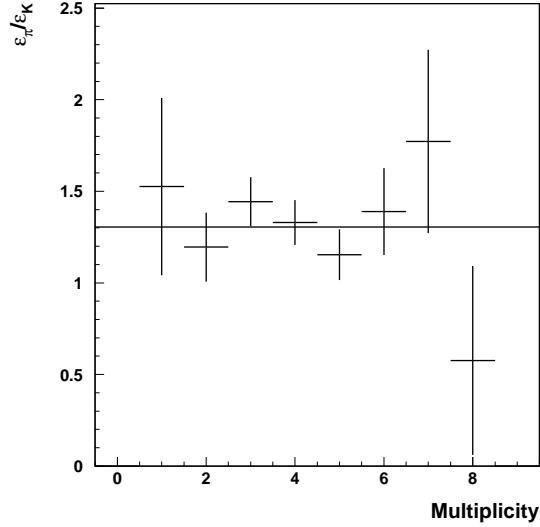


FIG. 5: Efficiency ratio for $D^0 \rightarrow \pi^- \ell^+ \nu / D^0 \rightarrow K^- \ell^+ \nu$ generic MC events as a function of multiplicity (number of additional mesons). The solid line is the result of a fit to a constant.

relative BRs	this analysis	PDG [5]	theor. pred. [22]
$\frac{\text{BR}(D^0 \rightarrow K^- e^+ \nu)}{\text{BR}(D^0 \rightarrow K^- \mu^+ \nu)}$	$1.002 \pm 0.041_{\text{stat}} \pm 0.048_{\text{syst}}$	1.12 ± 0.08	1.03
$\frac{\text{BR}(D^0 \rightarrow \pi^- e^+ \nu)}{\text{BR}(D^0 \rightarrow \pi^- \mu^+ \nu)}$	$1.20 \pm 0.18_{\text{stat}} \pm 0.09_{\text{syst}}$		1.02
$\frac{\text{BR}(D^0 \rightarrow \pi^- e^+ \nu)}{\text{BR}(D^0 \rightarrow K^- e^+ \nu)}$	$0.0809 \pm 0.0080_{\text{stat}} \pm 0.0032_{\text{syst}}$	0.101 ± 0.018	0.086
$\frac{\text{BR}(D^0 \rightarrow \pi^- \mu^+ \nu)}{\text{BR}(D^0 \rightarrow K^- \mu^+ \nu)}$	$0.0677 \pm 0.0078_{\text{stat}} \pm 0.0047_{\text{syst}}$		0.087

TABLE IV: Relative branching ratios

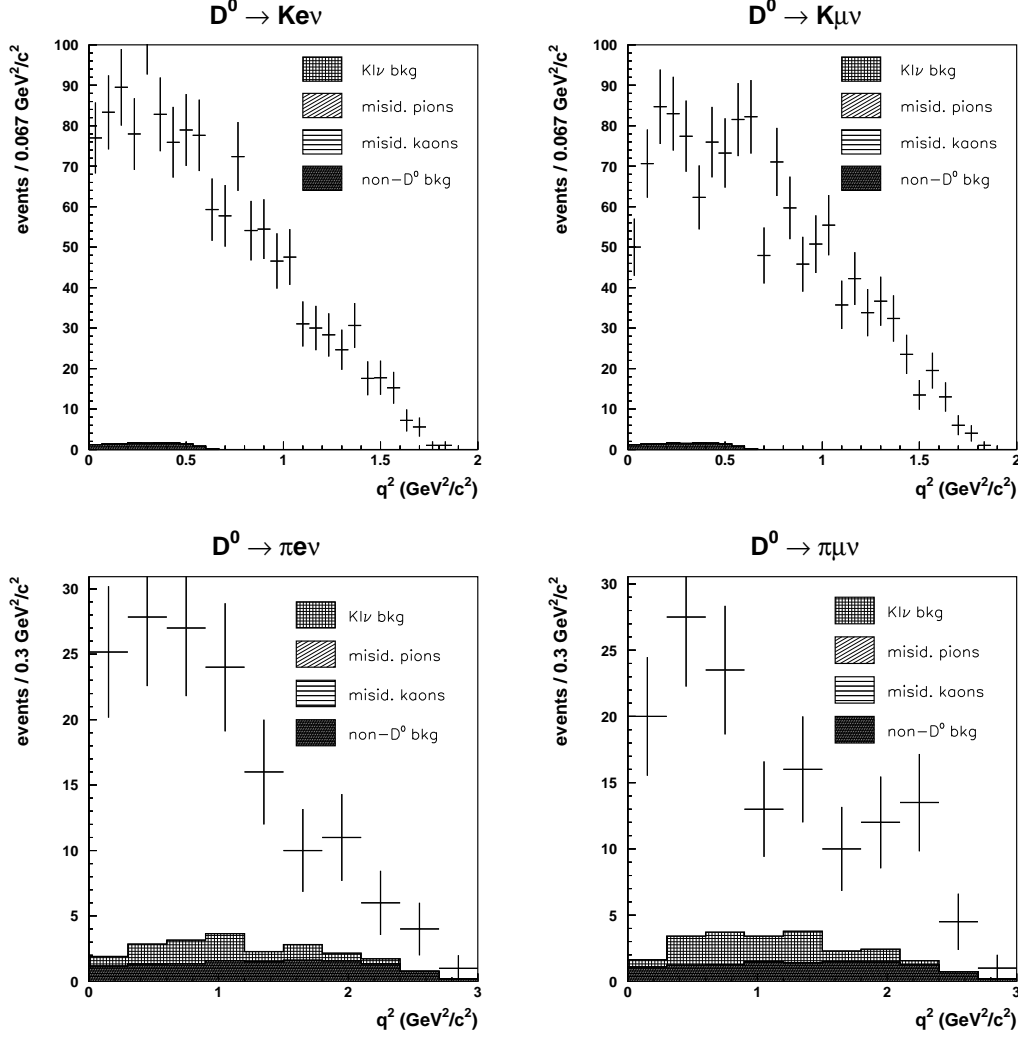


FIG. 6: q^2 distributions for $D^0 \rightarrow K^- e^+ \nu$ (upper left), $D^0 \rightarrow K^- \mu^+ \nu$ (upper right), $D^0 \rightarrow \pi^- e^+ \nu$ (lower left) and $D^0 \rightarrow \pi^- \mu^+ \nu$ (lower right), with contributions of individual background sources shown as histograms.

SEMILEPTONIC FORM FACTOR FOR $D^0 \rightarrow \pi^- \ell^+ \nu$ AND $D^0 \rightarrow K^- \ell^+ \nu$

In general, for $P \rightarrow P$ transitions (P denoting a pseudo-scalar meson), two form factors $f_+(q^2)$ and $f_-(q^2)$ are needed [7]. In the case of semileptonic decays, the matrix element is dominated by the form factor f_+ ; the influence of f_- is suppressed kinematically to a negligible (small) level for electrons (muons) by the smallness of m_l^2 compared to the scales of m_D^2 , p_π^2 and q^2 . Up to order m_l^2 one has

$$\frac{d\Gamma(D^0 \rightarrow \pi^- \ell^+ \nu)}{dq^2} = \frac{G_F^2 |V_{cd}|^2}{24\pi^3} |f_+(q^2)|^2 p_\pi^3 \quad (2)$$

and an analogous expression for $D^0 \rightarrow K^- \ell^+ \nu$, where p_π is the magnitude of the pion 3-momentum in the D^0 rest frame [25], determining the *kinematical weight* of the form factor.

These form factors have been calculated recently in unquenched lattice QCD [2], [4]. Earlier calculations were done in quenched lattice QCD [1], which works best in the region of high q^2 where measurements unfortunately suffer from poor statistics. In the *pole model* [7], the form factor f_+ is described as

$$f_+(q^2) = \frac{f_+(0)}{(1 - q^2/m_{\text{pole}}^2)} \quad (3)$$

with the pole masses $m_{D_s^*} = 2.11 \text{ GeV}/c^2$ (for $D^0 \rightarrow K^- \ell^+ \nu$) and $m_{D^*} = 2.01 \text{ GeV}/c^2$ (for $D^0 \rightarrow \pi^- \ell^+ \nu$).

Within the *modified pole model* [22], the form factor is given by

$$f_+(q^2) = \frac{f_+(0)}{(1 - q^2/m_{\text{pole}}^2)(1 - \alpha_p q^2/m_{\text{pole}}^2)}. \quad (4)$$

The ISGW2-model [8] predicts the following expression for the form factor:

$$f_+(q^2) = \frac{f_+(q_{\text{max}}^2)}{(1 - \alpha_I(q^2 - q_{\text{max}}^2))^2} = \frac{f_+(0)(1 + \alpha_I q_{\text{max}}^2)^2}{(1 - \alpha_I(q^2 - q_{\text{max}}^2))^2} \quad (5)$$

where q_{max}^2 is the kinematical limit of q^2 and α_I is a parameter of the model.

The normalized, bin-by-bin background subtracted and efficiency corrected q^2 distributions are shown in Fig. 7 for different decay modes; error bars indicate the sum in quadrature of statistical and systematic uncertainties. We fit the measured distributions to the predicted normalized differential decay width $\frac{1}{\Gamma} \frac{d\Gamma}{dq^2}$ of different models described above. Binning effects are accounted for by averaging the model functions over individual q^2 bins. Parameters $f(0)$ and $f(q_{\text{max}}^2)$ cancel out in the normalized decay width.

The fit results for the simple pole model with the pole mass as free parameter are shown in Fig. 7, left. The fitted pole masses are

$$m_{\text{pole}}(D^0 \rightarrow K^- e^+ \nu) = 1.88 \pm 0.06 \pm 0.03 \text{ GeV}/c^2 \quad (6)$$

$$m_{\text{pole}}(D^0 \rightarrow K^- \mu^+ \nu) = 1.77 \pm 0.04 \pm 0.03 \text{ GeV}/c^2 \quad (7)$$

$$m_{\text{pole}}(D^0 \rightarrow \pi^- e^+ \nu) = 2.01 \pm 0.13 \pm 0.04 \text{ GeV}/c^2 \quad (8)$$

$$m_{\text{pole}}(D^0 \rightarrow \pi^- \mu^+ \nu) = 1.92 \pm 0.09 \pm 0.04 \text{ GeV}/c^2 \quad (9)$$

where the first error is statistical and second systematic (discussed below). The χ^2/ndf values for fits using different models are shown in Table V. Values of $m_{\text{pole}}(K\ell\nu)$ are several standard deviations below the $m_{D_s^*}$. The pole mass for the $\pi\ell\nu$ decay agrees within errors with the predicted value, m_{D^*} . The fitted pole masses are also in agreement with results from CLEO [9] and FOCUS [10].

A fit to the modified pole model is also performed, where m_p is fixed to the theoretical pole $m_{D_{(s)}^*}$. The results for the fit parameter α_p are:

$$\alpha_p(D^0 \rightarrow K^- e^+ \nu) = 0.40 \pm 0.12 \pm 0.09 \quad (10)$$

$$\alpha_p(D^0 \rightarrow K^- \mu^+ \nu) = 0.66 \pm 0.11 \pm 0.09 \quad (11)$$

$$\alpha_p(D^0 \rightarrow \pi^- e^+ \nu) = 0.03 \pm 0.27 \pm 0.13 \quad (12)$$

$$\alpha_p(D^0 \rightarrow \pi^- \mu^+ \nu) = 0.19 \pm 0.32 \pm 0.16 \quad (13)$$

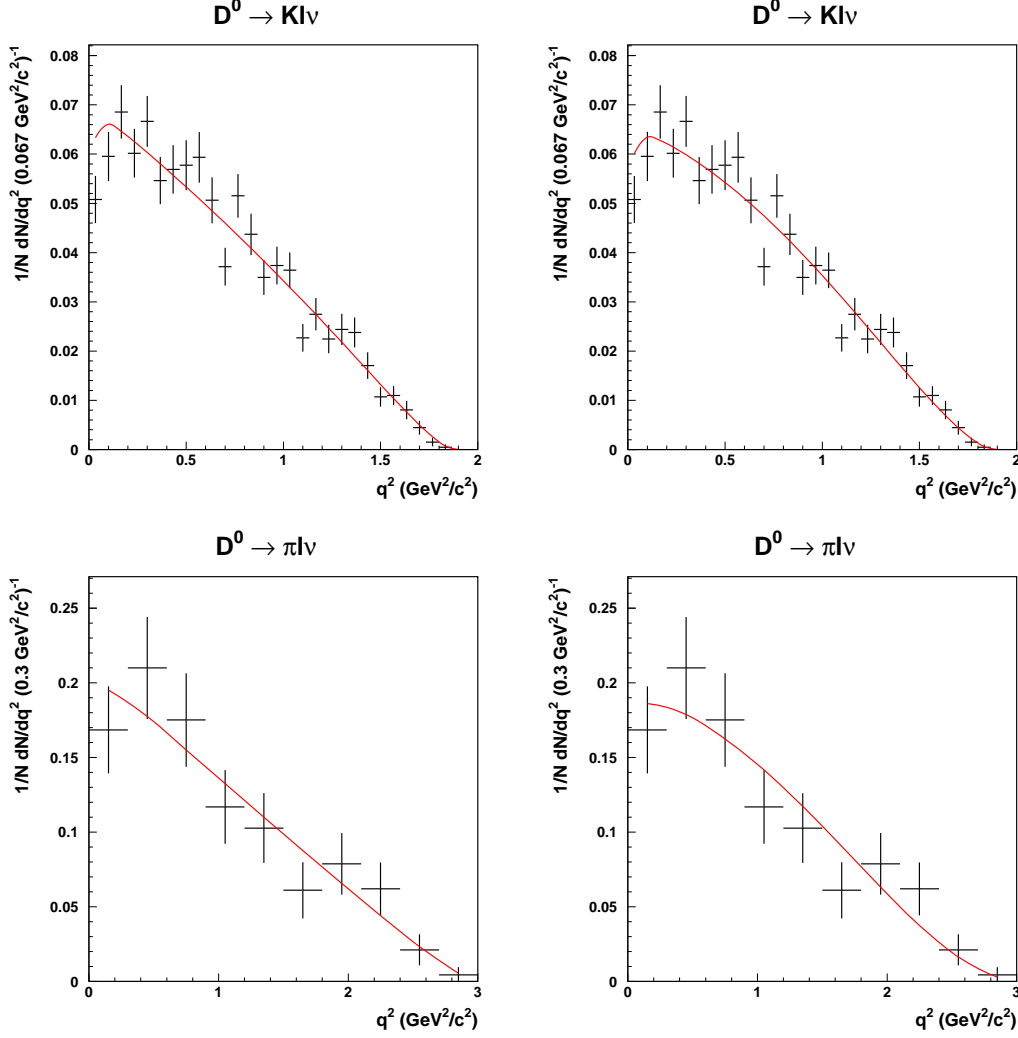


FIG. 7: Fraction of events in different q^2 -bins for $D^0 \rightarrow K^- \ell^+ \nu$ and $D^0 \rightarrow \pi^- \ell^+ \nu$ compared with the fits of the simple pole model (left) and ISGW2 (right)

Significantly non-zero values of $\alpha_p(K\ell\nu)$ suggest further contributions to the form factor, apart from the single pole at $m_{D_s^*}$.

Finally, a fit of the parameter α_I in the ISGW2 model yields (Fig. 7, right)

$$\alpha_I(D^0 \rightarrow K^- e^+ \nu) = 0.37 \pm 0.03 \pm 0.02 \text{ GeV}^{-2} c^2 \quad (14)$$

$$\alpha_I(D^0 \rightarrow K^- \mu^+ \nu) = 0.44 \pm 0.03 \pm 0.02 \text{ GeV}^{-2} c^2 \quad (15)$$

$$\alpha_I(D^0 \rightarrow \pi^- e^+ \nu) = 0.35 \pm 0.08 \pm 0.04 \text{ GeV}^{-2} c^2 \quad (16)$$

$$\alpha_I(D^0 \rightarrow \pi^- \mu^+ \nu) = 0.40 \pm 0.10 \pm 0.03 \text{ GeV}^{-2} c^2. \quad (17)$$

The χ^2 of the fit to the ISGW2 model is comparable to that for the two other models (c.f. Table V). The prediction of [8] for the $K\ell\nu$ mode is $\alpha_I = 0.47$, which is within one standard deviation of the $K\mu\nu$ result, and almost three standard deviations from the $Ke\nu$ result.

To study systematic uncertainties in different fits, each fit was repeated 50000 times, with the individual background normalizations varied within their Gaussian errors in a

χ^2/ndf	$K^-e^+\nu$	$K^-\mu^+\nu$	$\pi^-e^+\nu$	$\pi^-\mu^+\nu$
simple pole model	1.08	1.40	0.37	0.85
modified pole model	1.05	1.35	0.37	0.89
ISGW2	1.02	1.33	0.35	1.09

TABLE V: χ^2 per degree of freedom for fits to various models

correlated manner for all q^2 bins. The mean differences from the results of default fits were taken as systematic errors. A similar procedure was adopted to estimate the error due to the uncertainty on the q^2 dependent efficiency. The systematic error is included in the fit results above.

The absolute (i.e. not normalized) partial decay width is related to observable quantities by

$$\frac{d\Gamma(D^0 \rightarrow (\pi/K)^-\ell^+\nu)}{dq^2} = \frac{\epsilon_K BR_K N(q^2)}{\tau_D \epsilon_{q^2} N_K} \quad (18)$$

where ϵ_K , BR_K and N_K are the average efficiency, branching fraction, and number of reconstructed signal events in the $D^0 \rightarrow K^-\ell^+\nu$ mode, respectively. The world average value [5] is used for the branching fraction, as well as for the D^0 lifetime τ_D . ϵ_{q^2} and $N(q^2)$ are the efficiencies and signal yields in individual q^2 bins. A comparison of the measured values with lattice calculations [2] is shown in Fig. 8 (left). The uncertainty of the lattice results is mainly systematic (errors given in [2] are statistical only; relative systematic errors of about 10% were added in quadrature according to [3]). The lattice results in Ref. [4] are very similar to those in Ref. [2], and are therefore not shown here.

From the absolute partial decay width, also the absolute form factor can be extracted using Eqn. 2. Comparison of the measured values and lattice calculations [2] is shown in Fig. 8 (right). In order to make a more direct comparison, $f_+(q^2)$ is also calculated at the same q^2 values where the prediction is available. For interpolation we use the modified pole model (also used in [2]) with α_p obtained from the fit to data described above.

Using the integrated form of Eqn. 2 we determine the ratio of the form factors for $K\ell\nu$ and $\pi\ell\nu$ decay modes at $q^2 = 0$. For the q^2 dependence of the form factor we use the modified pole model with the values of parameter α_p in Eqn. 10-13, with the weighted average of K and π modes calculated taking into account correlated systematic errors. A similar averaging procedure is done for the measured ratios of branching fractions (Table IV). We measure the ratio

$$\frac{f_+(D^0 \rightarrow \pi^-\ell^+\nu)^2 |V_{cd}|^2}{f_+(D^0 \rightarrow K^-\ell^+\nu)^2 |V_{cs}|^2} \Big|_{q^2=0} = 0.041 \pm 0.003_{\text{stat}} \pm 0.004_{\text{syst}} \quad (19)$$

which is consistent within errors with the model-independent result using only the data in the first $\pi\ell\nu$ q^2 bin ($q^2 < 0.3 \text{ GeV}^2/c^2$). A recent theoretical prediction for the ratio [2] is 0.040 ± 0.004 .

This result is in fair agreement with those from CLEO [9] and FOCUS [20], which measure slightly lower values.

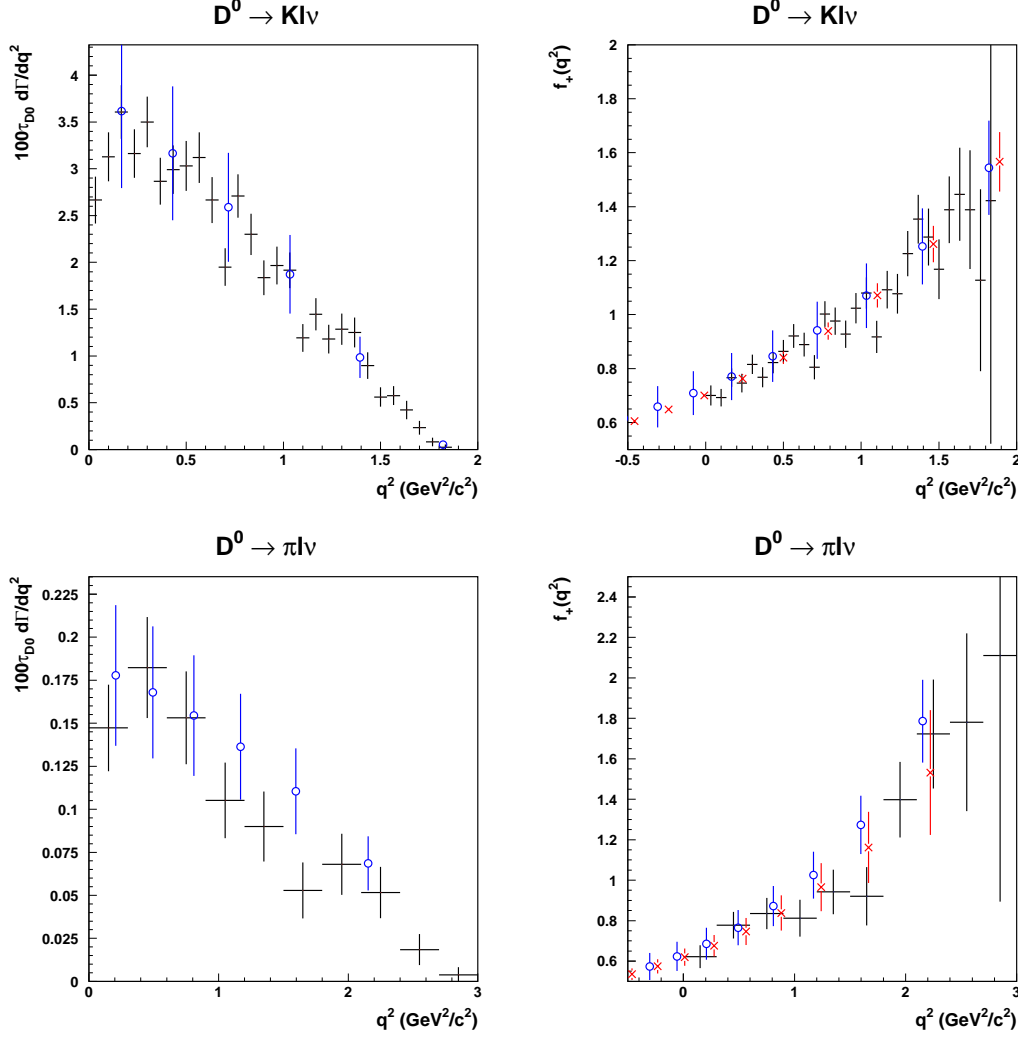


FIG. 8: Left plot: comparison of the absolute partial decay width $d\Gamma/dq^2$ with a lattice calculation (circles); right plot: comparison of the measured form factor (error bars) and unquenched lattice results (circles). To make a more direct comparison, $f_+(q^2)$ is also calculated at the same q^2 values where the lattice prediction is available (shifted slightly higher to avoid overlap), using the modified pole model with α_p parameter from the fit to the data (crosses)

SUMMARY AND CONCLUSIONS

In the present measurement we use fully reconstructed $e^+e^- \rightarrow D_{tag}^{(*)} D_{signal}^{*\pm} n h$ events ($h = \pi^{\pm 0}, K^{\pm}$), where the tag-side decay channels were $D^* \rightarrow D\pi, D\gamma$ and $D \rightarrow K^{\pm} n \pi$, $n = 1 - 3$ and the signal side was reconstructed from the recoil as $D^{*\pm} \rightarrow D^0 \pi^{\pm}$ and $D^0 \rightarrow K/\pi^- \ell^+ \nu$, $l = e, \mu$. Mass constraints at each reconstruction step enabled a very good resolution for the momentum transfer q^2 of $\sigma_{q^2} \sim 0.01 \text{ GeV}^2/c^2$.

We determined relative branching fractions

$$\frac{\text{BR}(D^0 \rightarrow \pi^- e^+ \nu)}{\text{BR}(D^0 \rightarrow K^- e^+ \nu)} = 0.0809 \pm 0.0080_{\text{stat}} \pm 0.0032_{\text{syst}} \quad (20)$$

$$\frac{\text{BR}(D^0 \rightarrow \pi^- \mu^+ \nu)}{\text{BR}(D^0 \rightarrow K^- \mu^+ \nu)} = 0.0677 \pm 0.0078_{\text{stat}} \pm 0.0047_{\text{syst}} \quad (21)$$

in good agreement with other measurements. The normalized measured q^2 distribution was fitted to different models of form factors. In the $K\ell\nu$ decay mode, where the sample of events with higher statistics is selected, some significant deviations from the predictions of the simple pole and ISGW2 model are observed. The results of the fit to the pole masses are $m_{\text{pole}}(K^- \ell^+ \nu) = 1.81 \pm 0.03 \pm 0.02 \text{ GeV}/c^2$ and $m_{\text{pole}}(\pi^- \ell^+ \nu) = 1.95 \pm 0.07 \pm 0.03 \text{ GeV}/c^2$. Using the measured values of the branching fraction ratio and the modified pole model with fitted parameter α_p , we obtain

$$f_+(D^0 \rightarrow \pi^- \ell^+ \nu)^2 / f_+(D^0 \rightarrow K^- \ell^+ \nu)^2 \cdot |V_{cd}|^2 / |V_{cs}|^2|_{q^2=0} = 0.041 \pm 0.003_{\text{stat}} \pm 0.004_{\text{syst}}. \quad (22)$$

in agreement with recent measurements [9, 20]. The form factors $f(q^2)$, obtained using the measured $d\Gamma/dq^2$ distribution and the world average of the $\text{Br}(D^0 \rightarrow K\ell\nu)$, are in nice agreement with the predictions of the recent unquenched lattice QCD results [2].

Acknowledgment

We very much appreciate the suggestions of the theoreticians T. Onogi and S. Hashimoto who provided the original motivation for this work. We thank the KEKB group for the excellent operation of the accelerator, the KEK cryogenics group for the efficient operation of the solenoid, and the KEK computer group and the National Institute of Informatics for valuable computing and Super-SINET network support. We acknowledge support from the Ministry of Education, Culture, Sports, Science, and Technology of Japan and the Japan Society for the Promotion of Science; the Australian Research Council and the Australian Department of Education, Science and Training; the National Science Foundation of China under contract No. 10175071; the Department of Science and Technology of India; the BK21 program of the Ministry of Education of Korea and the CHEP SRC program of the Korea Science and Engineering Foundation; the Polish State Committee for Scientific Research under contract No. 2P03B 01324; the Ministry of Science and Technology of the Russian Federation; the Ministry of Higher Education, Science and Technology of the Republic of Slovenia; the Swiss National Science Foundation; the National Science Council and the Ministry of Education of Taiwan; and the U.S. Department of Energy.

-
- [1] A. El-Khadra, A. Kronfeld, P. Mackenzie, S. Ryan, J. Simone, Phys. Rev. **D64**, 114004 (2001) [hep-ph/0101023].
 - [2] M. Okamoto *et al.*, Nucl. Phys. Proc. Suppl. **129**, 334(2004).
 - [3] M. Okamoto, private communication.
 - [4] C. Aubin *et al.*, (Fermilab Lattice Collaboration, MILC Collaboration and HPQCD Collaboration), Phys. Rev. Lett. **94**, 011601(2005). [hep-ph/0408306].
 - [5] F. J. Gilman, K. Kleinknecht and B. Renk, 2004 Review of Particle Properties, S. Eidelman *et al.*, Phys. Lett. **B592**, 1 (2004).
 - [6] G. Burdman, Z. Ligeti, M. Neubert, and Y. Nir, Phys. Rev. **D49** (1994) 2331.
 - [7] G. Armoros, S. Noguera, J. Portoles, Eur. Phys. J. **C27**, 243 (2003) [hep-ph/0109169].

- [8] N. Isgur and D. Scora, Phys. Rev. **D52**, 2783 (1995).
- [9] G. S. Huang *et al.*, (CLEO), Phys. Rev. Lett. **94**, 011802(2005) [hep-ex/0407035].
- [10] J. M. Link *et al.*, (FOCUS), Phys.Lett. **B607**, 233 (2005) [hep-ex/0410037].
- [11] M. Ablikim *et al.*, (BES), Phys. Lett. **B597**, 39(2004) [hep-ex/0406028].
- [12] Y. Gao *et al.*, (CLEO-c), [hep-ex/0408077].
- [13] A.Abashian *et al.*, (Belle), Nucl.Instr.Meth.**A479**, 117 (2002).
- [14] Y. Ushiroda *et al.*, Nucl.Instr.Meth.**A511**, 6 (2003).
- [15] see <http://www.lns.cornell.edu/public/CLEO/soft/QQ>.
- [16] R. Brun *et al.*, GEANT 3.21, CERN Report DD/EE/84-1, 1984.
- [17] T. Uglov *et al.*, (Belle), Phys. Rev. **D70**, 071101 (2004).
- [18] K. Abe *et al.*, (Belle), Phys. Rev. **D66**(2002) 032007.
- [19] K. Hanagaki *et al.*, Nucl. Instrum. Meth. **A 485**(2002) 490.
- [20] J. M. Link *et al.*, (FOCUS), Phys.Lett. **B607**, 51 (2005) [hep-ex/0410068].
- [21] S. Blusk *et al.*, [hep-ex/0505035].
- [22] D. Becirevic, A.B. Kaidalov, Phys. Lett. B 478, 417 (2000).
- [23] The slightly higher wrong-sign background in the uds -component can be understood as an effect of charge conservation: the expected correlation of n charges under the constraint of charge conservation, *i.e.*, a net charge of zero, but otherwise uncorrelated, is $\langle Q_i Q_j \rangle = -1/(n - 1)$, which averages for the uds -sample to -0.14 ± 0.03 compared to an observed correlation in the uds D^0 background of -0.16 ± 0.01 .
- [24] In the first case, the π^+ is misidentified as lepton; in the second case, the K^- is misidentified as lepton.
- [25] For our analysis, we use the full formula of Ref. [7], including m_l^2 terms, which gives a small correction for low q^2 values.